Optical Interconnection Using VCSELs and Polymeric Waveguide Circuits

Takashi Sakamoto, Hiroyuki Tsuda, *Member, IEEE, Member, OSA*, Makoto Hikita, *Member, IEEE*, Toshiaki Kagawa, *Member, IEEE*, Kouta Tateno, and Chikara Amano, *Member, IEEE, Member, OSA*

***Abstract*—We investigated the waveguide loss and transmission characteristics for optical interconnection using vertical-cavity surface-emitting lasers (VCSELs) and multimode polymeric waveguide circuits with crossings. The excess loss with 100 crossings is 2.2 dB when the image magnification from a VCSEL to a waveguide is 2.3. We obtained error-free (i.e., bit error rate $<10^{-11}$) optical interconnection at 1.0625 Gbps regardless of the number of crossings or the magnification. These results suggest the practicality of large-scale optical interconnection between VCSEL-based smart-pixel chips using multimode waveguides with more than 100 crossings.**

***Index Terms*—Optical interconnection, smart pixel, vertical-cavity surface-emitting laser (VCSEL), waveguide.**

I. Introduction

ELECTRICAL interconnects are reaching their inherent limits in terms of operating speed, packaging, and power dissipation in multichip modules (MCMs) with CMOS chips. Optical interconnects in and between chips have a high potential to overcome these limits [1]. Recently, smart-pixel chips, which include optical I/O and electrical signal processing circuits, have been proposed [2]. In particular, there have been many reports on smart-pixel chips in which vertical-cavity surface-emitting lasers (VCSELs) are integrated as optical elements [3]-[5]. This is because of the advantages VCSELs offer which include symmetrical beam profiles with small beam divergence, the availability of two-dimensional arrays, high-speed modulation, and low power consumption.

The approaches for forming optical interconnects between smart-pixel chips include the use of free-space [6], waveguides [7], and fiber bundles [8]. We have proposed optical interconnection between VCSEL-based smart-pixel chips by planar waveguide circuits with crossings [9]. A waveguide link is suitable for optical interconnection between VCSEL-based smart-pixel chips on a single substrate because any smart-pixel chip at any location on the substrate can be connected to any other smart-pixel chip with a single planar waveguide circuit with $45°$ mirrors. In particular, multimode waveguides are useful as optical interconnects between smart-pixel chips because they offer a larger optical coupling tolerance.

Fig. 1 shows the model of the 128 input $\times$ 128 output optical switch proposed in this study. The switch consists of 16 input $\times$ 16 output banyan switch smart-pixel chips and a multimode planar waveguide circuit. The direction of the light launched into the waveguide from a VCSEL is changed by 90° with a 45° mirror. The light propagates throughout the straight and curved waveguide and traverses the many crossings. On the opposite side of the waveguide, the direction of the light is changed by 90° with the other 45° mirror. The light is eventually received by a photodetector (PD). The mirror loss was estimated to be 0.2 to 0.8 dB at 0.83 μm and the 12 mm-waveguide loss with S-shape curve of 6 mm radius was 0.9 dB [10].

In the system shown in Fig. 1, at most 98 crossings occur in one optical link between a VCSEL and a PD, where such crossings also cause optical loss. Since the PD needs a certain minimum amount of optical power, the number of crossings in the link is inherently limited by optical loss. And the loss value per crossing depends on the optical intensity distribution in the core. So the loss value depends on the VCSEL field pattern and the magnification M, defined as the ratio of the image size at the input edge of the waveguide to the VCSEL radiative size.

In such a multimode system, modal noise, which is a random fluctuation in the received light intensity, is caused by the interference between propagating modes in the waveguides and by mode-selective loss (MSL) in the link [11]. The modal noise occurring at the optical interconnection between VCSEL-based smart-pixel chips by multimode waveguides should be suppressed to achieve error-free interconnects.

In this paper, we investigate the dependence of the waveguide loss and transmission characteristics on the number of crossings in the waveguides and the image magnification from a VCSEL to the waveguide. We also discuss the possibility of optical interconnection between smart-pixel chips with VCSELs by using multimode waveguides with crossings.

II. Experimental

Fig. 2 is a schematic of the experimental setup used in this study. We used a 0.85-μm VCSEL as input and multimode polymeric waveguides with crossings. The VCSEL consisted of a C-doped p-type $Al_{0.9}Ga_{0.1}As$–$Al_{0.15}Ga_{0.85}As$ distributed Bragg reflector (DBR) (37.5 pairs), multiple quantum wells (MQW) active region, and a Si-doped n-type $Al_{0.9}Ga_{0.1}As$–$Al_{0.15}Ga_{0.85}As$ DBR (23 pairs), which were grown on a p–GaAs substrate [12]. The device is an etched-mesa

Manuscript received May 15, 2000; revised August 7, 2000.

T. Sakamoto, T. Kagawa, K. Tateno, and C. Amano are with NTT Photonics Laboratories, Kanagawa 243-0198, Japan.

H. Tsuda was with NTT Photonics Laboratories, Kanagawa 243-0198, Japan. He is now with the Department of Electronics and Electrical Engineering, Keio University,

M. Hikitawas with NTT Photonics Laboratories, Ibaraki 319-1193, Japan. He is now with the Technology Development Center, NEE Advanced Technology Corporation, Ibaraki, 319–1193, Japan.

Publisher Item Identifier S 0733-8724(00)09824-8.

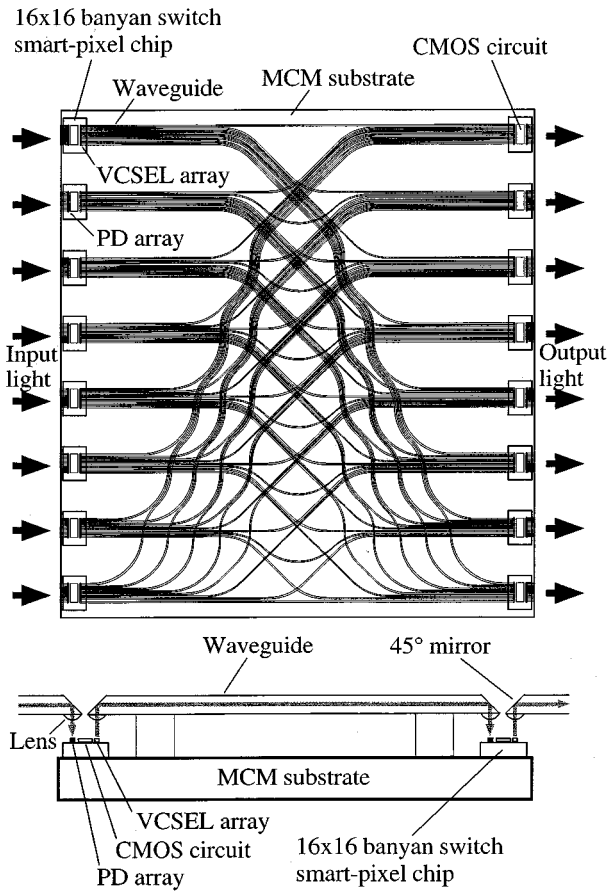

Fig. 1. Model of the 128 input × 128 output optical switch MCM.

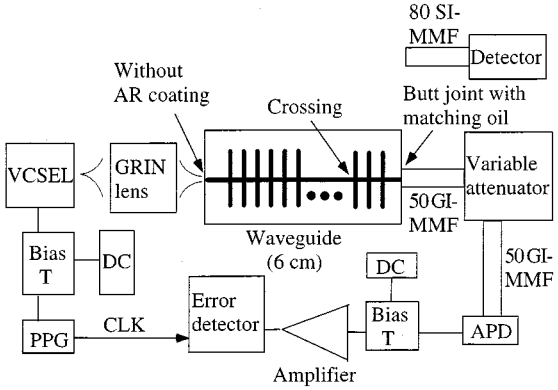

Fig. 2. Experimental setup.

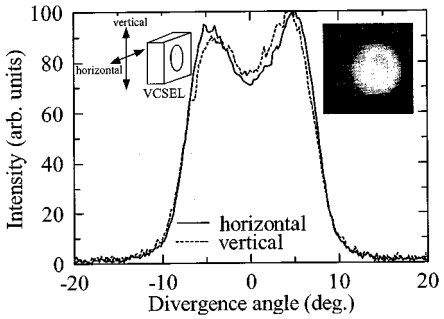

Fig. 3. VCSEL far field pattern at $I = 18$ mA. Full width at half maximum (FWHM) is about 15°. The inset shows the near field pattern at $I = 18$ mA. Scales are arbitrary.

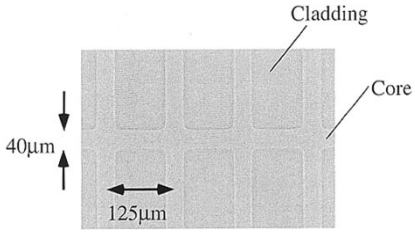

Fig. 4. Micrograph of a polymeric waveguide with crossings.

type and has an active diameter of 15 μm. Polyimide was used for lateral current confinement and optical confinement. Fig. 3 shows the far-field patterns (FFPs) and the near-field pattern (NFP) at 18 mA (the threshold current, I_{th}, is around 9 mA). It is clear that the device oscillates in several transverse modes. The VCSEL chip was mounted on a gold-coated copper heatsink using Au–Sn metal. The n-electrode of the VCSEL chip and the contact pad on the heatsink were connected with 25-μm-diameter gold wire. Fig. 4 shows a micrograph of the polymeric waveguide with crossings. The cross angle is 90° and the separation between the crossings is 125 μm. Deuterated poly-methylmethacrylate (d-PMMA) was used for the waveguide core and UV curable epoxy resin for the cladding [13]. The refractive indexes of the core and cladding were 1.489 and 1.471 at 0.83 μm, respectively. The relative index difference between them was 1.2% and the numerical aperture, NA, was 0.229, which corresponds to the maximum input angle of 13.2°. The width and height of the core were 40 and 42.5μm, respectively. The propagation loss of the straight waveguides was less than 0.02 dB/cm at 0.85 μm. These waveguides were 6-cm long with 0–100 crossings.

The output light of the VCSEL was coupled into an antireflection (AR)-coated graded-index (GRIN) rod lens with a 0.29 pitch, and the light from the lens was focused on the core of the waveguide end. When the magnification was between 0.7–2.6, the spot size on the waveguide end was smaller than the waveguide core size and the numerical aperture (NA) of the waveguide was larger than the incident angle from the GRIN lens, such that the coupling loss, excluding Fresnel reflection loss, was negligible.

For the propagation loss measurement, the VCSEL was biased to 18 mA ($2\times I_{th}$). The output light from the waveguide was launched into a 1-m-long 80/125 step-index multimode fiber (SI–MMF). The core of the fiber was larger than that of the polymeric waveguide, and index profile of the fiber was step-like, so we considered the coupling loss to be negligible. To avoid Fresnel reflection, we placed matching oil between the waveguide and the fiber.

To measure the transmission characteristics, the VCSEL was biased up to 1.4 times the I_{th}, and modulated directly by a pulse pattern generator (PPG). The PPG generated a $2^{23} - 1$ PRBS NRZ signal at a bit rate of 1.0625 Gbps. We set the peak-to-peak voltage V_{pp} at 0.6 V. The bias current and the modulation signal from the PPG were combined in a bias tee. The lower level of the driving signal input into the VCSEL was nearly equal to the threshold. We launched the output light from the waveguide into a 50/125 graded-index multimode fiber (GI–MMF)

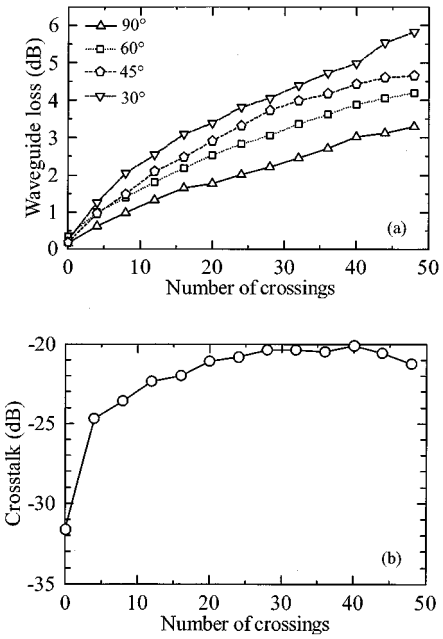

Fig. 5. (a) Waveguide loss as a function of the number of crossings and the crossing angle when a 50/125 GI-MMF pigtailed 850-nm DFB-LD with a mode scrambler is used. (b) Crosstalk to the neighboring waveguide as a function of the number of crossings, where the waveguide separation is 250 μm and the crossing angle is 90°.

with matching oil and detected it using a 2-GHz-bandwidth Si-avalanche photodiode (APD). Then the signal was amplified electrically and fed to an error detector.

III. Results and Discussion

A. Angle Dependence

To clarify the optimal crossing angle, we investigated the cross-angle dependence of the waveguide loss. In Fig. 5 (a), the waveguide loss is shown as a function of the number of crossings and the crossing angle, where the optical transmitter was a 50/125 GI-MMF pigtailed 850-nm DFB-LD with a mode scrambler and the waveguide was 3-cm long and designed to have 0–48 crossings with a 250-μm separation. The crossing angles were 30°, 45°, 60°, or 90°. The loss was lowest for 90° crossing angles. Consequently, crossing angle was maintained at 90° in subsequent experiments.

In Fig. 5 (b), the crosstalk to the neighboring waveguide is also shown as a function of the number of crossings. The waveguide separation was 250 μm and the crossing angle 90°. Other conditions were the same as described for Fig. 5 (a). The crosstalk saturated at around -20 dB.

B. Waveguide Loss

Fig. 6 shows the waveguide loss with and without 100 crossings as a function of the magnification M. The experimental configurations for $M = 1$ and $M = 2$ are illustrated in the inset of Fig. 6. Without crossings, the waveguide loss, which is the sum of the propagation loss and the coupling loss, was constant at approximately 0.5 dB. By contrast, the waveguide loss with 100 crossings decreased monotonically as the magnification increased. Let $L_{\mathrm{with}}(M, N)$, $L_{\mathrm{without}}(M)$,

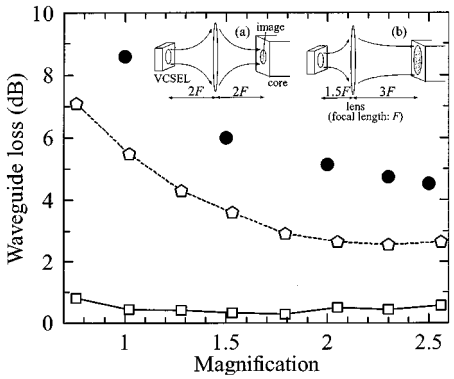

Fig. 6. Magnification dependence of waveguide loss. Solid line: without crossings (straight waveguide). Dashed line: with 100 crossings. Filled circles: calculation with 100 crossings (assuming waveguide loss without crossings is 0.5 dB). The inset shows the optical coupling between a VCSEL and waveguide when (a) $M = 1$ and (b) $M = 2$.

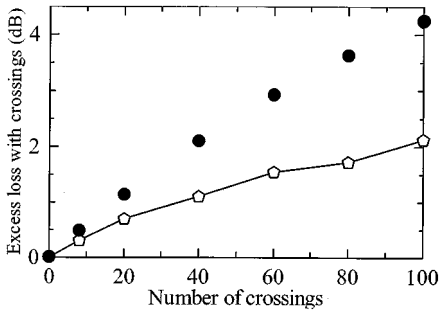

Fig. 7. Dependence of excess loss with crossings on the number of crossings when $M = 2.3$. Solid line: experiments. Filled circles: calculation.

and $L_{\mathrm{excess}}(M, N) = L_{\mathrm{with}}(M, N) - L_{\mathrm{without}}(M)$ be the propagation loss with N crossings, that without crossings, and the excess loss with N crossings, respectively. The difference between the two lines in the figure is equivalent to the excess loss with 100 crossings, $L_{\mathrm{excess}}(M, N = 100)$. One of the lowest values of $L_{\mathrm{excess}}(M, N = 100)$ is $L_{\mathrm{excess}}(M = 2.3, N = 100)$, 2.2 dB. As described later, this level is sufficiently low for application to the interconnection of over 100 crossings. It is clear that the excess loss with crossings decreased as M increased. Fig. 7 shows the excess loss with crossings as a function of the number of crossings N when $M = 2.3$. As N increased, the excess loss per crossing decreased. The experimental results in Fig. 6 and 7 indicate that the excess loss with crossings is mode-selective loss (MSL). These results will be compared with calculations below.

Our interpretation that the excess loss with crossings is MSL is justified by the FFP and NFP measurements. The FFPs of waveguides without crossings and with 100 crossings are shown in Fig. 8 (a) and (b), respectively (the current $I = 7.0$ mA, and $M = 1$). The full width at half maximum (FWHM) of the horizontal FFP of the waveguide without crossings was broader than that of the waveguides with 100 crossings (8.6° and 6.0°, respectively). By contrast, the FWHM of the vertical FFP without crossings and that of the waveguide with 100 crossings were the same (12.6°). These results indicate that the loss at crossings is mode-selective (lower-mode pass filter). The NFPs of the waveguide are shown in the insets of Fig. 8. The NFP in Fig. 8 (a),

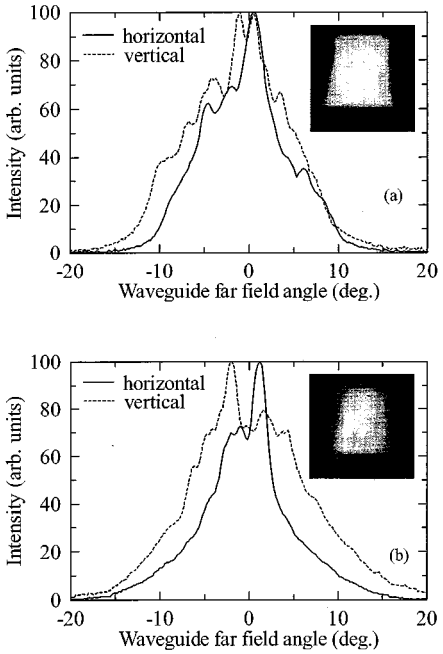

Fig. 8. Waveguide far field patterns under the condition of $M = 1$ and $I = 7$ mA. (a) Without crossings, (b) with 100 crossings. Intensity is normalized by the maximum intensity. The insets show the waveguide near field patterns under the same condition. Scales are arbitrary.

which was obtained with $M = 1$ and $I = 7$ mA without crossings, shows an almost uniform distribution. On the other hand, the NFP in Fig. 8 (b), where $M = 1$ and $I = 7$ mA with 100 crossings, shows peaks of intensity near the center of the core. These results suggest that higher order modes are easily lost at crossings. These FFP and NFP measurements strongly support our interpretation.

C. Transmission Characteristics

Fig. 9 shows typical eye diagrams measured on a digitizing oscilloscope at 1.0625 Gbps with and without 100 crossings when $M = 1$ or $M = 2.3$. The eyes are open in all cases. Fig. 10 shows the measured bit error rate (BER) curves when $M = 1$ and $M = 2.3$. The reference curve is for a configuration where a DFB-LD, LN modulator, and APD were connected using optical fibers without a lens and waveguides. We achieved error-free transmission under all conditions. Regardless of the number of crossings and the magnification, the lines show penalties of approximately 2 dB at BER $= 10^{-11}$. BER floors were not observed. The penalty when $M = 2.3$ was slightly larger than that when $M = 1$, probably because the optical coupling for $M = 2.3$ was more easily influenced by mechanical noise in the measurement.

D. Discussion

In this section we discuss the dependence of the excess loss with crossings on the number of crossings and magnification using a geometrical-optics model. Because the waveguide's core is much larger than the wavelength, we can use an approximate geometrical-optics description. We performed the calculations using the number of crossings in the waveguides $N = 0 - 100$, length $L = 6$ cm, and core width and height

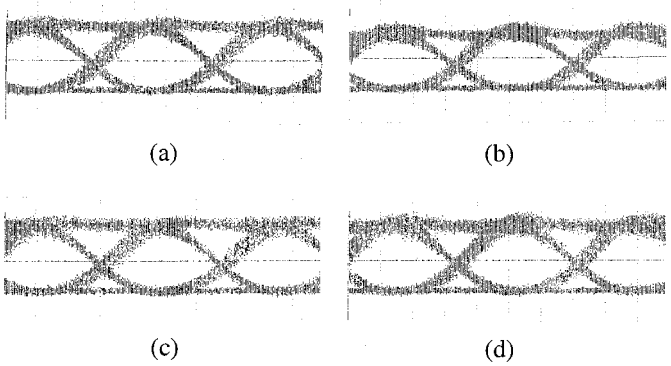

Fig. 9. 1.0625-Gbps eye diagrams. (a) $M = 1$ without crossings. (b) $M = 1$ with 100 crossings. (c) $M = 2.3$ without crossings. (d) $M = 2.3$ with 100 crossings.

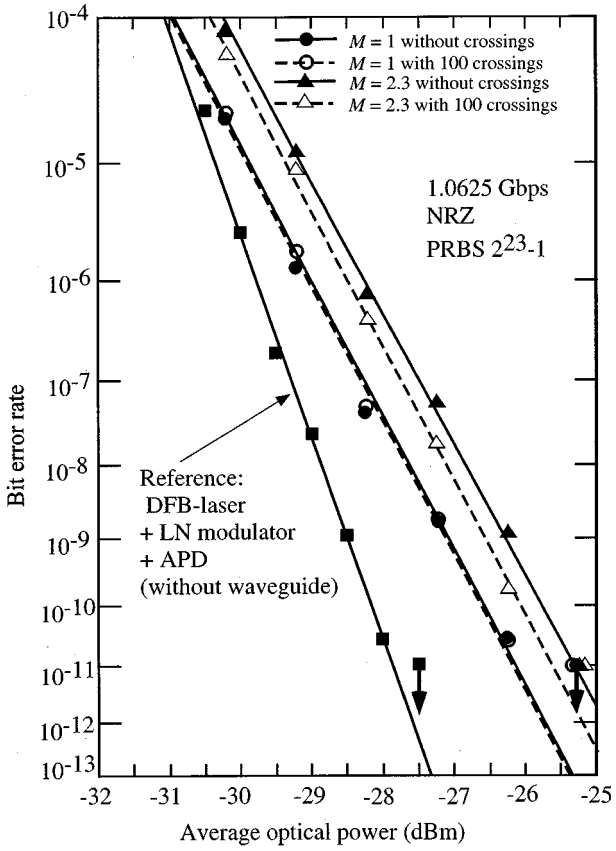

Fig. 10. BER characteristics at 1.0625 Gbps.

$W = 40$ μm. A light beam forms an angle θ with the z axis (optical axis), and the projection of the light beam on the x–y plane forms an angle t with the x axis, as shown in Fig. 11. The light beam represented by the solid line travels in the core. By contrast, for the light beam represented by the dashed line, there is no total internal reflection at the core-cladding interface because of the crossings. This light beam does not travel in the core and results in the excess loss with the crossings. The probability that a light beam is not reflected totally at a sidewall is WN/L; therefore, the probability that a light beam is reflected totally at the sidewall is $1 - WN/L = (L - WN)/L$. The number of times the light beam (θ, t) is totally reflected at the sidewalls is $L/W/(\tan\theta \cos t) = L \tan\theta \cos t/W$. The

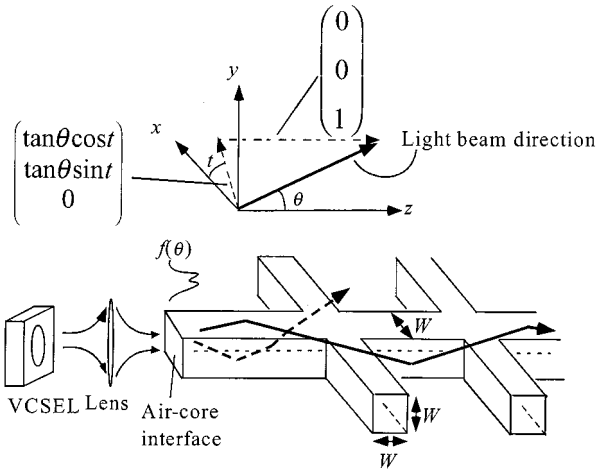

Fig. 11. Geometrical-optics model of crossing loss.

probability that a light beam (θ, t) is not lost on the way is $\{(L - WN)/L\}^{L \tan\theta \cos t/W}$. Hence, the proportion of light beams not lost on the way, P, is

$$P = \frac{\displaystyle\int_{\theta=0}^{\theta=\pi/2}\int_{t=0}^{t=\pi/2} f(\theta)\left(\frac{L-WN}{L}\right)^{(L\tan\theta\cos t/W)} d\theta dt}{\displaystyle\int_{\theta=0}^{\theta=\pi/2}\int_{t=0}^{t=\pi/2} f(\theta)\, d\theta dt} \tag{1}$$

where $f(\theta)$ is the intensity distribution just after the light passes through the air-core interface. Fig. 6 shows the magnification dependence of the waveguide loss with 100 crossings, which we calculated using the measured FFP of the VCSEL (Fig. 3), Snell's law of refraction at the air-core interface, and the formula $1/D_0 + 1/MD_0 = 1/F$ (F: focal length, D_0: distance between light source and lens, and M: magnification). Here, we assumed that the waveguide loss without crossings is 0.5 dB (the waveguide loss with crossings is the sum of the waveguide loss without crossings and the excess loss with crossings). Similar to the experimental results, this plot indicates that, as the magnification increases, the excess loss with crossings decreases. This is because the larger the magnification becomes, the smaller the angle of the light beams becomes, so the number of reflections at the core-cladding interface decreases. The simulation of the dependence of the excess loss with crossings on the number of crossings for $M = 2.3$ is summarized in Fig. 7. As clearly seen in the figure, the crossing number dependence of the excess loss is not linear, which is also similar to the experimental results. This is because light beams of higher modes are attenuated in the crossings located in the initial stage.

Finally, we evaluated the capacity of the switch using optical interconnection between smart-pixel chips with waveguides. The total loss should be suppressed to within an acceptable level determined by the VCSEL output power and PD characteristics. If we assume the coupling loss at both a VCSEL and a PD to be 3 dB, the bending loss in a link to be 4 dB at most, and the acceptable total loss to be 15 dB, the acceptable crossing loss is 5 dB at maximum. As clarified above, the loss of 100 crossings is about 2.2 dB. This suggests that the switch shown in Fig. 1 is a practical model. In a k input $\times$ k output switch with 16 input $\times$ 16 output banyan switch smart-pixel chips, the maximum number of crossings in one link is $(k - 16)^2/k$. For a 256 input $\times$ 256 output optical switch using 16 input $\times$ 16 output banyan switch smart-pixel chips, there are at most 225 crossings between a VCSEL and a PD. Since the loss of 100 crossings is about 2.2 dB, we estimate the loss of 225 crossings to be lower than 5 dB, which suggests that a 256 input $\times$ 256 output optical switch is still practical.

IV. Conclusion

With the goal of achieving optical interconnection between VCSEL-based smart pixels with a planar multimode waveguide circuit, we investigated the dependence of waveguide loss and transmission characteristics on the number of crossings in the waveguides and image magnification from a VCSEL to the waveguide. From the loss dependence on both the magnification and the number of crossings, we clarified that crossing loss is mode-selective loss. This interpretation is justified by FFP and NFP measurements and a geometrical-optics model. The excess loss with 100 crossings is about 2.2 dB, which is low enough to achieve the interconnection of more than 100 optical ports. We have also demonstrated error free (BER $< 10^{-11}$) optical interconnection at 1.0625 Gbps, regardless of the number of crossings and image magnification. These results suggest the practical feasibility of a large-scale optical interconnect between VCSEL-based smart-pixel chips with a planar multimode waveguide circuit, such as a 256 input $\times$ 256 output optical switch.

Acknowledgment

The authors thank Drs. T. Nakahara and H. Uenohara for helpful discussions, and Drs. H. Iwamura and S. Imamura for their encouragement.

References

[1] G. Verschaffelt, R. Buczynski, P. Tuteleers, P. Vynck, V. Baukens, H. Ottevaere, C. Debaes, S. Kufner, M. Kufner, A. Hermanne, J. Genoe, D. Coppee, R. Vounckx, S. Borghs, I. Veretennicoff, and H. Thienpont, "Demonstration of a monolithic multichannel module for multi-Gb/s intra-MCM optical interconnects," *IEEE Photon. Technol. Lett.*, vol. 10, pp. 1629–1631, Nov. 1998.

[2] S. Matsuo, T. Nakahara, K. Tateno, and T. Kurokawa, "Novel technology for hybrid integration of photonic and electronic circuits," *IEEE Photon. Technol. Lett.*, vol. 8, pp. 1507–1509, Nov. 1996.

[3] T. Nakahara, H. Tsuda, K. Tateno, S. Matsuo, and T. Kurokawa, "Hybrid integration of smart pixels by using polyimide bonding: Demonstration of a GaAs p-i-n photodiode/CMOS receiver," *IEEE J. Select. Topics Quantum Electron.*, vol. 5, pp. 209–216, Mar. 1999.

[4] R. Pu, C. Duan, and C. W. Wilmsen, "Hybrid integration of VCSELs to CMOS integrated circuits," *IEEE J. Select. Topics Quantum Electron.*, vol. 5, pp. 201–208, Mar. 1999.

[5] A. V. Krishnamoorthy, L. M. F. Chirovsky, W. S. Hobson, R. E. Leibenguth, S. P. Hui, C. J. Zydzik, K. W. Goosen, J. D. Wynn, B. J. Tseng, J. Lopata, J. A. Walker, J. E. Cunningham, and L. A. D'Asaro, "Vertical-cavity surface-emitting lasers flip-chip bonded to gigabit-per-second CMOS circuits," *IEEE Photon. Technol. Lett.*, vol. 11, pp. 128–130, Jan. 1999.

[6] N. McArdle, M. Naruse, and M. Ishikawa, "Optoelectronic parallel computing using optically interconnected pipelined processing arrays," *IEEE J. Select. Topics Quantum Electron.*, vol. 5, pp. 250–260, Mar. 1999.

[7] R. T. Chen, L. Wu, L. Lin, C. Choi, Y. Liu, B. Bihari, S. Tang, R. Wickman, B. Picor, and Y. S. Liu, "Guided-wave Si CMOS process-compatible optical interconnects," in *Proc. Semiconductor Conf.*, vol. 2, Oct. 1999, pp. 467–471.
[8] A. Neyer, B. Wittmann, and M. Jöhnck, "Plastic-optical-fiber-based parallel optical interconnects," *IEEE J. Select. Topics Quantum Electron.*, vol. 5, pp. 193–200, Mar. 1999.
[9] H. Tsuda, T. Sakamoto, M. Hikita, T. Nakahara, K. Tateno, T. Kagawa, C. Amano, and T. Kurokawa, "Hybrid-integrated smart pixels for MCM and board-level optical interconnects," in *Tech. Dig. Opt. Comput.*, CO, Apr. 1999, OFA1, pp. 212–214.
[10] M. Hikita, R. Yoshimura, A. Kaneko, M. Usui, S. Tomaru, and S. Imamura, "Free-standing polymeric optical waveguide films for optical interconnections," in *Proc. ECOC'97*, vol. 2, Edinburgh, UK, Sep. 1997, pp. 285–288.
[11] D. M. Kuchta and C. J. Mahon, "Mode selective loss penalties in VCSEL optical fiber transmission links," *IEEE Photon. Technol. Lett.*, vol. 6, pp. 288–290, Feb. 1994.
[12] Y. Kohama, Y. Ohiso, K. Tateno, and T. Kurokawa, "0.85-μm vertical-cavity surface-emitting laser diode arrays grown on p-type GaAs substrate," *IEEE Photon. Technol. Lett.*, vol. 9, pp. 280–281, Mar. 1997.
[13] R. Yoshimura, M. Hikita, S. Tomaru, and S. Imamura, "Very low loss multimode polymeric optical waveguides," *Electron. Lett.*, vol. 33, no. 14, pp. 1240–1242, Jul. 1997.

Takashi Sakamoto received the B.S. and M.S. degrees from the University of Tokyo, Tokyo, Japan, in 1994 and 1996, respectively.

In 1996, he joined NTT Optoelectronics Laboratories, Kanagawa, Japan, where his interests are photonic networks.

Mr. Sakamoto is a member of the Institute of Electronics, Information, and Communications Engineers (IEICE) of Japan and the Japan Society of Applied Physics.

Hiroyuki Tsuda (M'99) was born in Tokyo, Japan, on February 28, 1962. He received the B. S. degree from Waseda University, Japan, in 1885, the M. E. and Ph.D. degrees from Tokyo Institute of Technology, Japan, in 1987 and 1998, respectively.

In 1987, he joined NTT Opto-electronics Laboratories, Kanagawa, Japan where he was initially engaged in research on nonlinear optical devices including a nonlinear etalon and a bistable laser diode. In 1994, he was engaged in development of 10 Gbit/s transmission systems. Since 1996, he has been researching on smart pixels with vertical cavity surface emitting lasers and on time-to-space conversion optical signal processing using an arrayed-waveguide grating. Since 2000 he has been at the Department of Electronics and Electrical Engineering, Keio University, where he is now an Assistant Professor.

Dr. Tsuda is a member of the Institute of Electronics, Information and Communication Engineers of Japan, the Japan Society of Applied Physics, the Optical Society of Japan, and the Optical Society of America.

Makoto Hikita (M'98) was born in Tokyo, Japan, on December 3, 1950. He received the B.E. and M.E. degrees in instrumentation engineering from Keio University in 1973 and 1975, respectively, and the Ph. D. degree in physics from Osaka University in 1990.

In 1975, He joined NTT Musashino Labolatories, Tokyo, where he was engaged in resarch on superconducting telecommunication cables. In 1977, he moved to NTT Ibaraki Laboratories where he was engaged in research on superconducting materials, Josephson devices, Anderson Localization and superconducting physics. From 1992, he has been engaged in the development of electro-optic and passive polymer optical component devices. He is presently a Senior Research Engineer at NTT Optoelectronics Laboratories.

Dr. Hikita is a member of The Institute of Electronics, Information and Communication Engineers in Japan, The Physical Society of Japan, The Society of Polymer Science of Japan and The Japan Society of Applied Physics.

Toshiaki Kagawa (M'91) was born in Kanagawa, Japan, on October 22, 1952. He received the B.S., M.S., and Ph. D. degrees in physics from Tokyo Institute of Technology, Tokyo, Japan, in 1975, 1977, and 1985, respectively.

In 1977, he joined NTT Electrical Communication Laboratories, Tokyo. He engaged in research and development of amorphous semiconductors, superlattice avalanche photodiodes, and vertical surface emitting laser diodes. He was a Visiting Scientist with the Max-Planck-Institute, Germany, from 1993 to 1994.

Dr. Kagawa is a member of Japan Society of Applied Physics and Institute of Electronics, Information, Communication Institute.

Kouta Tateno was born in Tochigi, Japan, on January 25, 1968. He received the B.S. and the M.S. degrees in the chemistry from the University of Tokyo, Tokyo, Japan, in 1991 and 1993, respectively. In 1993, he joined NTT Optoelectronics Laboratories, where he became engaged in research of the III-V crystal growth for optical devices.

Mr. Tateno is a member of the Japan Society of Applied Physics.

Chikara Amano (M'94) received the B.S. and M.S. degrees in physics from Tokyo University, Tokyo, Japan in 1980 and 1982, respectively, and the Ph.D. degree from Tokyo Institute of Technology, Japan, in 1990.

Since joining NTT Laboratories, Japan, in 1982, he has been engaged in research on several epitaxial growth techniques of III-V compound semiconductors, such as MBE, MOCVD, and CBE, and the design and fabrication of optoelectronic devices such as lasers, modulators, detectors, their integrated switch devices, and solar cells. He is now a group leader of parallel signal processing research group in NTT Photonics Laboratories, Kanagawa, Japan.

Dr. Amano is a member of the IEEE Lasers and Electrooptics Society, the Optical Society of America, and the Institute of Electronics, Information and Communication Engineers of Japan.